

ISTANBUL TECHNICAL UNIVERSITY ★ GRADUATE SCHOOL OF SCIENCE
ENGINEERING AND TECHNOLOGY

**FABRICATION OF AN ELECTROCHEMICAL BIOSENSOR FOR
DETECTION OF DOPAMINE, EMPLOYING TYROSINASE IMMOBILIZED
POLYMERIC NANOFIBERS**

M.Sc. THESIS

Uğur DAĞLI

Department of Nanoscience and Nanoengineering

Nanoscience and Nanoengineering Programme

JANUARY 2015

ISTANBUL TECHNICAL UNIVERSITY ★ GRADUATE SCHOOL OF SCIENCE
ENGINEERING AND TECHNOLOGY

**FABRICATION OF AN ELECTROCHEMICAL BIOSENSOR FOR
DETECTION OF DOPAMINE, EMPLOYING TYROSINASE IMMOBILIZED
POLYMERIC NANOFIBERS**

M.Sc. THESIS

**Uğur DAĞLI
(513121012)**

Department of Nanoscience and Nanoengineering

Nanoscience and Nanoengineering Programme

Thesis Advisor: Prof. Dr. A. Sezai SARAÇ

JANUARY 2015

İSTANBUL TEKNİK ÜNİVERSİTESİ ★ FEN BİLİMLERİ ENSTİTÜSÜ

**TİROZİNAZ BAĞLI POLİMERİK NANOFİBERLER KULLANILARAK
DOPAMİN TAYİNİ İÇİN ELEKTROKİMYASAL BİYOSENSÖR ÜRETİMİ**

YÜKSEK LİSANS TEZİ

**Uğur DAĞLI
(513121012)**

Nanobilim ve Nanomühendislik Anabilim Dalı

Nanobilim ve Nanomühendislik Programı

Tez Danışmanı: Prof. Dr. A. Sezai SARAÇ

OCAK 2015

Uğur DAĞLI, a **M.Sc.** student of **ITU Graduate School of Science Engineering and Technology** student ID **513121012**, successfully defended the **thesis** entitled **“FABRICATION OF AN ELECTROCHEMICAL BIOSENSOR FOR DETECTION OF DOPAMINE, EMPLOYING TYROSINASE IMMOBILIZED POLYMERIC NANOFIBERS”**, which he prepared after fulfilling the requirements specified in the associated legislations, before the jury whose signatures are below.

Thesis Advisor : **Prof. Dr. A. Sezai SARAÇ**
Istanbul Technical University

Jury Members : **Doç. Dr. Fatma Neşe KÖK**
Istanbul Technical University

Prof. Dr. Yücel ŞAHİN
Yildiz Technical University

Date of Submission : 15 December 2015

Date of Defense : 21 January 2015

To my family,

FOREWORD

I would like to express my sincere appreciation and thanks to my supervisor, Prof. Dr. A.Sezai SARAÇ for his continuous encouragement, guidance, motivation and immense knowledge.

I am also thankful to my colleagues Selin GÜMRÜKÇÜ, Burcu SAYINLI, Samin DASTJERD, Zeliha GÜLER, Timuçin BALKAN, Deniz GÜLERCAN, Ash GENÇTÜRK, and Mehmet Giray ERSÖZOĞLU for their collaborative and friendly manner.

I would especially like to thank my friends Rıdvan ERGUN, Ayşegül DEVELİOĞLU, Ekin EŞEN, Ömercan SUSAM and İpek KURU for the fun and quality time.

Lastly, and most importantly, I wish to thank my family to whom I dedicate this thesis as a token of my gratitude.

January 2015

Uğur DAĞLI

TABLE OF CONTENTS

	<u>Page</u>
FOREWORD	ix
TABLE OF CONTENTS	xi
ABBREVIATIONS	xiii
LIST OF TABLES	xv
LIST OF FIGURES	xvii
SUMMARY	xix
ÖZET	xxi
1. INTRODUCTION	1
2. THEORETICAL PART	4
2.1 Conductive Polymers in Biosensor Applications	4
2.2 Electrospinning	5
2.2.1 Effects of various parameters on electrospinning process	5
2.2.1.1 Concentration	5
2.2.1.2 Molecular weight	6
2.2.1.3 Viscosity	6
2.2.1.4 Surface tension	6
2.2.1.5 Conductivity / surface charge density	6
2.2.1.6 Applied voltage	7
2.2.1.7 Feed rate / flow rate	7
2.2.1.8 Tip to collector distance	7
2.3 Dopamine	7
2.4 Electrochemical Impedance Spectroscopy in Biosensor Applications	8
2.5 Basic Principles and Terms in Impedance Spectroscopy	10
3. EXPERIMENTAL PART	12
3.1 Materials	12
3.2 Preparation of PAN/PU/P3ANA Blends	12
3.3 Electrospinning of PAN/PU/P3ANA	12
3.4 Covalent Immobilization of Tyrosinase onto Nanofiber Mats	13
3.5 Quantification of the Protein Amount on the Nanofiber Mats	13
3.6 Structural, Morphological and Electrochemical Characterization	14
4. RESULTS AND DISCUSSION	Error! Bookmark not defined.
4.1 Spectroscopic Characterization of Nanofibers	15
4.2 Determination of Immobilized Enzyme Amount by BCA Assay	18
3.1 Morphological Characterization of Nanofibers	19
3.2 Electrochemical Impedance Spectroscopy and Equivalent Circuit Modelling	22
5. CONCLUSION	28
REFERENCES	29
CURRICULUM VITAE	37

ABBREVIATIONS

BCA	: Bicinchoninic acid
DMF	: Dimethylformamide
EDX	: Energy Dispersive X-ray Spectroscopy
EIS	: Electrochemical Impedance Spectroscopy
FTIR	: Fourier Transform Infrared Spectroscopy
IUPAC	: International Union of Pure and Applied Chemistry
PAN	: Polyacrylonitrile
PBS	: Phosphate Buffer Saline
PU	: Polyurethane
P3ANA	: Poly(m-anthranilic acid)
SEM	: Scanning Electron Microscope
Tyr	: Tyrosinase
UV-Vis	: Ultraviolet Visible Spectrophotometer

LIST OF TABLES

	<u>Page</u>
Table 4.1 : Elemental concentrations for nitrogen and copper atoms in PAN/PU/P3ANA nanofibers and tyrosinase immobilized nanofibers....	22
Table 4.2 : Fitting values for the equivalent circuit elements by the simulation of the impedance spectra in Figure 4.9.	26

LIST OF FIGURES

	<u>Page</u>
Figure 1.1 : Schematic representation of fabrication of PAN/PU/P3ANA nanofibers by electrospinning (a), and immobilization of tyrosinase onto nanofiber mat by EDC/NHS activation (b).	3
Figure 2.1 : Sequence of enzymatic reactions generating other catecholamines from L-DOPA.	8
Figure 2.2 : Impedance expressed as the modulus $ Z $ and the phase angle ϕ , or specified by the real (Z_R) and imaginary (Z_I) parts.	10
Figure 2.3 : Randles' equivalent circuit for an electrode in contact with an electrolyte.....	11
Figure 4.1 : UV-Vis spectra of PAN, PU, P3ANA and PAN/PU/P3ANA.....	15
Figure 4.2 : FTIR spectra of PAN/PU/P3ANA blend with increasing P3ANA amounts.....	16
Figure 4.3 : FTIR-ATR spectra of tyrosinase immobilized PAN/PU/P3ANA nanofibers.....	17
Figure 4.4 : Amount of initial and residual tyrosinase after each immobilization step.....	19
Figure 4.5 : SEM images of PAN/PU (a), and PAN/PU/P3ANA nanofibers containing 0.075 g (b), 0.150 g (c), and 0.300 g (d) of P3ANA.....	20
Figure 4.6 : SEM images of PAN/PU/P3ANA nanofibers (a) and 0.5 mg (b) and 2 mg (c) of tyrosinase immobilized nanofibers..	21
Figure 4.7 : EDX-mapping of nitrogen (red) and copper (Blue) atoms on the surface of tyrosinase immobilized PAN/PU/P3ANA nanofibers.	21
Figure 4.8 : Nyquist (A), and Bode Phase (B) plots indicating that measured and calculated data well fitted to each other with the model.....	23
Figure 4.9 : Equivalent circuits for the simulation of the EIS spectra of PAN/PU/P3ANA nanofibers (top) and tyrosinase immobilized PAN/PU/P3ANA nanofibers (bottom).	24

FABRICATION OF AN ELECTROCHEMICAL BIOSENSOR FOR DETECTION OF DOPAMINE, EMPLOYING TYROSINASE IMMOBILIZED POLYMERIC NANOFIBERS

SUMMARY

Nanofibers of polyacrylonitrile (PAN)/polyurethane (PU)/poly(*m*-anthranilic acid) (P3ANA) blend were fabricated by the electrospinning process. UV-Visible spectroscopy was performed to confirm the incorporation of each individual polymer into the nanofibers. This is followed by a Fourier Transform Infrared Spectroscopy – Attenuated Total Reflectance (FTIR-ATR) analysis, which displayed an increasing intensity in the bands specific to poly(*m*-anthranilic acid), in correlation with its increasing amounts in the blend. Nanofibers with the highest amount of P3ANA were then used for enzyme immobilization, considering it provides more carboxyl groups for enzymes to bind onto. Next, tyrosinase immobilization on these nanofibers was carried out by 1-ethyl-3-(dimethyl-aminopropyl) carbodiimide hydrochloride (EDC)/*N*-hydroxyl succinimide (NHS) activation procedure. Covalent binding of tyrosinase onto nanofiber mats was confirmed by FTIR-ATR analysis, and a subsequent bicinchoninic acid (BCA) assay revealed the amount of enzyme immobilized. Morphology and composition of nanofibers before and after enzyme immobilization were characterized by Scanning Electron Microscopy (SEM)/Energy Dispersive X-ray Spectroscopy (EDX). The surface morphology of the tyrosinase immobilized PAN/PU/P3ANA nanofibers became smoother and the diameters of the fibers increased. Elemental analyses and EDX-mapping of nitrogen and copper atoms showed that the enzyme was evenly distributed on the surface of the nanofibers. Then, Electrochemical Impedance Spectroscopy (EIS) analysis was performed to observe the effects of immobilized enzyme on electrochemical properties of nanofibers and the data were fitted with an equivalent electrical circuit model. The changes in structure, composition and morphology of nanofibers after tyrosinase immobilization affected their electrochemical behavior. The solution resistance and charge transfer resistance of nanofibers decreased after enzyme immobilization.

TİROZİNAZ BAĞLI POLİMERİK NANOFİBERLER KULLANILARAK DOPAMİN TAYİNİ İÇİN ELEKTROKİMYASAL BİYOSENSÖR ÜRETİMİ

ÖZET

Enzimler sahip oldukları yüksek katalitik etkinlik ve yüksek selektivite gibi özelliklerinden dolayı biyosensör, biyokataliz, biyoremediasyon, gıda prosesleri ve farmasötik sentez gibi birçok biyokimyasal uygulamada geniş kullanım alanı bulmaktadır. Fakat, düşük stabiliteleri ve geri kazanımlarındaki zorluklar enzimlerden yararlanılan çalışmalarda önemli bir sorun teşkil etmektedir. Bu sorunun üstesinden gelmeye yönelik bir çözüm olarak, özellikle son yıllarda, enzimlerin çözünmeyen katı destekler üzerine immobilizasyonu büyük önem kazanmıştır. Bu sayede enzimin geri kazanımını kolaylaştırmak ve dolayısıyla tekrar kullanılabilirliğini arttırmak hedeflenmektedir.

Enzim immobilizasyonu için katı destek olarak nanomalzemelerin kullanımı giderek daha da önem kazanmakta ve yaygınlaşmaktadır. Nanomalzemeler, özellikle sahip oldukları yüksek yüzey alanı/hacim oranının getirisi olarak enzim yükleme kapasitesini ve katalitik verimi büyük ölçüde arttırdığından dolayı tercih edilmektedir. Özellikle polimerik nanofiberler, diğer nanomalzemeler kullanıldığında karşılaşılabilen sınırlı kütle transferi ve elektrolitik çözeltide dispersiyona uğrama gibi sorunlara yol açmadığından nanomalzemeler arasında ön plana çıkmaktadır. Bunun yanı sıra, farklı özelliklere sahip polimer karışımları hazırlanarak, biyoyumluluk, iletkenlik ve mekanik güç gibi istenen niteliklerin biraraya getirildiği nanofiberler elde edilebilir ve bu şekilde sistem optimize edilebilir.

Kullanılan malzemenin elektriksel iletkenliği, özellikle biyosensör uygulamalarında büyük önem arz eder. Bu durum göz önünde bulundurularak, elektrokimyasal nitelikleriyle ön plana çıkan poli(m-antranilik asit) tercih edilmiştir. Poli(m-antranilik asit)'in sağladığı bir başka avantaj da enzimin kovalent bağlanabileceği serbest karboksil gruplarına sahip olmasıdır. Kullanılan bir diğer polimer olan poliakrilonitril de güçlü adezyon özelliğinden dolayı tercih edilmiştir. Poliüretan ile de nanofiberlerin mekanik gücünü arttırmak hedeflenmiştir. Bunun yanı sıra poliakrilonitril ve poliüretan, fiber oluşturmadaki üstün nitelikleriyle ön plana çıkmaktadır.

Bu çalışmada ilk olarak poliakrilonitril (PAN) ve poliüretan (PU) ağırlıkça 1:1 oranında karıştırılarak dimetilformamid (DMF) içerisinde ağırlıkça %6'lık homojen çözelti elde edildi. Aynı şekilde üç farklı çözelti daha hazırlanarak her birine sırasıyla 0.075 g, 0.150 g, vs 0.300 g poli(m-antranilik asit) (P3ANA) ilave edildi. Daha sonra bu polimer çözeltileri elektrospin yöntemiyle nanofiber üretiminde kullanıldı. Elde edilen nanofiberler ilk olarak ultraviyole (morötesi) ve görünür bölge spektroskopisiyle karakterize edildi. Her bir polimerin nanofiber yapısına katılımı UV -görünür bölge spektrumunda görüntülenen spesifik absorpsiyon bantları tarafından doğrulandı. Ardından yapılan Fourier dönüşümlü infrared (kızılötesi) (FTIR-ATR) spektroskopik analizi de poliakrilonitril, poliüretan ve poli(m-antranilik asit)'in spesifik absorpsiyon bantlarını görüntülemenin yanı sıra, farklı örneklerde

giderek artan poli(m-antranilik asit) miktarının yansıması olarak bu polimere ilişkin absorpsiyon bantlarının intensitesinde kademeli bir artış göstererek artan miktarlarda poli(m-antranilik asit)'in yapıya başarılı bir şekilde katıldığını onayladı.

Spektroskopik analiz sonrasında en yüksek miktarda (0.300 g) poli(m-antranilik asit) içeriğine sahip olan nanofiberler enzim immobilizasyonunda kullanılmak üzere alındı. Poli(m-antranilik asit)'in yapısında bulunan serbest karboksil grupları, enzimin yapısında bulunan amino grupları ile kovalent bağ oluşturarak enzim immobilizasyonunu sağladığından, yüksek miktarda poli(m-antranilik asit) içeriğinin enzim yükleme kapasitesini arttıracak dikkate alınarak en fazla poli(m-antranilik asit) içeriğine sahip olan nanofiberler tercih edildi. Enzimin (tirozinaz) kovalent immobilizasyonu için 1-etil-3-(dimetil-aminopropil) carbodiimid hidroklorid (EDC)/N-hidroksil süksinimid (NHS) aktivasyon presüdüğü uygulandı. Nanofiber matları, fosfat tampon tuzu (PBS) çözeltisinde (0.1 M, pH 7.4) 1:1 molar oranda karıştırılan EDC/NHS çözeltisine 2 saat boyunca maruz bırakılarak oda sıcaklığında 2 saat boyunca karıştırıldı. 2 saatin sonunda fiberler alınarak fazla EDC/NHS'i uzaklaştırmak üzere 2 defa PBS ile yıkandı ve bu şekilde aktive edilmiş olan fiberler bu kez biri 0.5 mg/mL, diğeri 2 mg/mL olan 2 farklı tirozinaz çözeltisine maruz bırakıldı. 4°C'de 2 saatlik inkübasyonun ardından fiberler yine 2 defa PBS ile yıkanarak kovalent bağlanmayan enzimlerin uzaklaştırılması sağlandı. Yıkamalardan arda kalan çözeltiler sonrasında enzim miktarının tayininde kullanılmak üzere alındı. Enzim immobilizasyonu bu şekilde gerçekleştirildikten sonra enzim bağlı nanofiber matlar ilk olarak FTIR-ATR spektroskopisiyle karakterize edildi. Oluştugu gözlenen yeni absorpsiyon bantları, daha önceki bantlarda gözlenen kaymalar ya da spesifik bantların intensitesindeki azalmalar, nanofiberlere tirozinazın bağlanmasından kaynaklanan yapısal değişiklikleri doğruladı. Tirozinazın kovalent bağlanması bu şekilde doğrulandıktan sonra, bağlı olan enzim miktarını tayin etmek üzere bikinkoninik asit (BCA) yöntemi uygulandı. Enzim bağlama ve sonrasındaki yıkama adımlarından arda kalan solüsyonlara BCA çalışma solüsyonu ilave edilerek 37°C'de 30 dakika inkübe edildi ve ardından UV-görünür bölge spektrofotometresi kullanılarak 562 nm'deki absorbans değerlerine bakıldı. Kovalent bağlanmayan enzimlerin ortamdan uzaklaştırılması sonucunda yıkama solüsyonlarında kalan tirozinaz miktarının giderek azaldığı gözlemlendi ve başlangıç solüsyonundaki enzimin %87'sinin kovalent bağlandığı hesaplandı.

Enzim immobilizasyon sürecinin başarıyla gerçekleştirildiği bu şekilde doğrulandıktan sonra nanofiberlerin morfolojik karakterizasyonuna geçildi. Taramalı elektron mikroskobu kullanılarak elde edilen görüntülerden nanofiber çapları PAN/PU blendi için 103 ± 11 nm, artan miktarlarda P3ANA içeren PAN/PU/P3ANA blendleri içinse sırasıyla 144 ± 24 nm (0.075 g P3ANA), 111 ± 17 nm (0.150 g P3ANA) ve 119 ± 22 nm (0.300 g P3ANA) olarak bulundu. PAN/PU blendine ait nanofiberler düzgün bir yüzey morfolojisine sahipken artan miktarlarda P3ANA içeren nanofiberlerin giderek daha pürüzlü bir yüzey morfolojisi sergilediği gözlemlendi. 0.5 mg ve 2 mg tirozinaz bağlanan nanofiberlerin çapları ise sırasıyla 131 ± 22 nm ve 141 ± 21 nm olarak ölçüldü. Nanofiber çaplarındaki artışların yanı sıra, enzim immobilizasyon sürecinin nanofiberlerin yüzey pürüzlülüğünü belirgin şekilde azalttığı gözlemlendi.

İmmobilize edilen tirozinazın nanofiberler üzerindeki dağılımını görüntülemek üzere, bir başka morfolojik karakterizasyon yöntemi olan enerji dağılımlı X-ışını spektroskopisi (EDX) uygulandı. Tirozinazın yapısında bulunan, ancak polimerik nanofiberlerin yapısında bulunmayan bakır atomunun dağılımına yönelik bu elemental analiz, doğrudan tirozinazın dağılımı hakkında bilgi sahibi olmaya olanak

tanıdı. Sonuçta tirozinazın nanofiberler üzerinde homojen dağılım gösterdiği, bu dağılımın özellikle P3ANA'nın yapısında bulunan karboksil gruplarının dağılımıyla örtüştüğü gözlemlendi.

Son olarak nanofiberlerin elektrokimyasal davranışları elektrokimyasal empedans spektroskopisiyle analiz edildi ve özellikle enzim immobilizasyonunun nanofiberlerin elektrokimyasal özelliklerini ne şekilde etkilediği karşılaştırmalı olarak incelendi. Nyquist ve Bode faz açısı grafiklerinden elde edilen deneysel veriler eşdeğer devre modelleri üzerinden değerlendirildi. Enzim içermeyen nanofiberlerin elektrot olarak, PBS'in ise elektrolit olarak kullanıldığı sistem $R(CR)(QR)W$ eşdeğer devresiyle tanımlandı. Bu eşdeğer devre tasarlanırken elektrolitten gelen çözelti direnci (R_s), çözeltiyle nanofiber yüzeyi arasındaki yük transfer direnci (R_{ct}), fiberler üzerindeki çift tabaka kapasitansı (C_{dl}), sabit faz elemanı (Q) ve Warburg empedansı göz önünde bulunduruldu. Tirozinaz immobilizasyonu sonrasında elde edilen sisteme karşılık gelen eşdeğer devre ise, nanofiberlerle çözelti arasına giren enzim tabakası ve bundan kaynaklanan yeni direnç ve kapasitans elemanları dikkate alınarak $R(CR)(CR)(QR)W$ şeklinde tanımlandı. Tirozinaz immobilizasyonu sonucunda arayüz yapısında meydana gelen değişikliklere bağlı olarak çözelti direnci ve yük transfer direncinde bir düşüş olduğu tespit edildi.

1. INTRODUCTION

Enzymes have received remarkable attention due to their versatile biochemical applications such as biocatalysis, biosensor fabrication, bioremediation, biofuel cells, food processing, and pharmaceutical synthesis [1-5]. Their intrinsic properties of high catalytic efficiency and high selectivity, which can differentiate between substrates, optical isomers, and similar regions of molecules, have made them indispensable biochemical tools [6-10]. However, their instability and non-reusability due to difficulty in recovery present some practical drawbacks. These drawbacks can be overcome by immobilizing the enzymes onto insoluble or solid supports, which prevents the undesirable conformational change of the enzymes and allows for easy recovery of the enzymes for reuse [1,11]. From this point of view, covalent immobilization of the probes by using reactive groups on the support material has been recognized as an attractive strategy since it provides the control of the immobilization of biological probes on the surface [12].

Utilizing nanostructured materials as supports for enzyme immobilization have recently proved to be a convenient method, considering their extremely high surface area to volume ratio which promotes an increased enzyme loading capacity and enhanced catalytic efficiency [11]. Among these nanostructured materials, electrospun nanofibers stand out as the better alternative because they eliminate the problem of limited mass transfer which is the case when mesoporous silica is used as a support, or the problem of recovery which is observed in the case of nanoparticle supports due to their dispersion in reaction solution. In addition to that, using polymeric nanofibers allows for further optimization of the nanofiber properties as there is a variety of electrospinnable polymers to meet different requirements such as biocompatibility, conductivity or mechanical strength [1]. Electrospinning is a simple, convenient, and versatile technique for generating nanofibers with desired properties [13].

Electrical conductivity is also a desirable property for the support material to have, especially in the electrochemical biosensor applications. Enhanced electron transfer

ability of the support makes the catalytic reaction of the enzyme sustainable [14-18]. Among the conductive polymers, polyaniline (PANI) and its derivatives are one of the most promising classes thanks to their well-defined electrochemical properties. However, the low processability due to their low solubility limits their usage [19-21]. In order to overcome this obstacle, aniline monomer was modified with alkyl side chains, sulfonic acid groups, or carboxyl groups [22]. Poly(m-anthranilic acid) (P3ANA) which has carboxylic acid group on the main aniline backbone, is a promising conductive polymer due to its solubility in aqueous and non-aqueous solvents as well as other polar solvents [19]. In addition to that, these free carboxyl groups (-COOH) makes it a very convenient choice for enzyme immobilization. However, fabrication of P3ANA nanofibers with electrospinning is not an easy task, which is the case for other conductive polymers as well. Therefore, P3ANA needs to be blended with another electrospinnable polymer.

Most recently, acrylonitrile-based polymers [13] and polyurethane (PU) [23] have been widely used for electrospinning due to their superior fiber-forming properties. Besides, polyacrylonitrile (PAN) exhibits good adhesive properties [24], whereas polyurethane has improved mechanical strength [25], which makes these two polymers good candidates for blending with P3ANA. Moreover, PAN is selected to blend with P3ANA for the formation of charge transfer complexes between the negatively charged functional groups ($-C\equiv N:$) and functional groups (-COOH) of P3ANA, leading to enhanced electrical properties and interfacial interactions between polymer chains [26].

In this study, tyrosinase (Tyr) was covalently immobilized onto polyacrylonitrile/polyurethane/ poly(m-anthranilic acid) (PAN/PU/P3ANA) nanofibers. Tyrosinase was chosen as a model enzyme because it is commercially widely available and it catalyzes versatile reactions. The purpose of covalent immobilization of tyrosinase was to incorporate a sensing biomolecule into the nanofiber mat, so as to endow them with a potential use in biosensor applications. Tyrosinase catalyzes the conversion of phenolic compounds, dopamine being one of them, so it can be employed as a specific biosensing element in varying fields from food processing to analyzing dopaminergic pathways in central nervous system. The activation of electrospun PAN/PU/P3ANA nanofiber mats for covalent enzyme immobilization was achieved by 1-ethyl-3-(dimethyl-aminopropyl) carbodiimide hydrochloride

(EDC)/N-hydroxyl succinimide (NHS) activation procedure (Figure 1.1). The amount of immobilized enzyme was determined by bicinchoninic acid (BCA) protein assay. Tyrosinase immobilized nanofiber mats were characterized spectroscopically (Fourier Transform Infrared - Attenuated Total Reflectance (FTIR-ATR) and UV-Vis spectrophotometer) and morphologically (SEM/EDX). The interaction between tyrosinase and carboxylic acid groups on the P3ANA was investigated by means of electrochemical impedance spectroscopy (EIS). Increasing amount of tyrosinase was successfully immobilized with covalent binding onto PAN/PU/P3ANA nanofibers. The charge transfer resistances of the enzyme immobilized nanofibers were decreased with increasing enzyme amount.

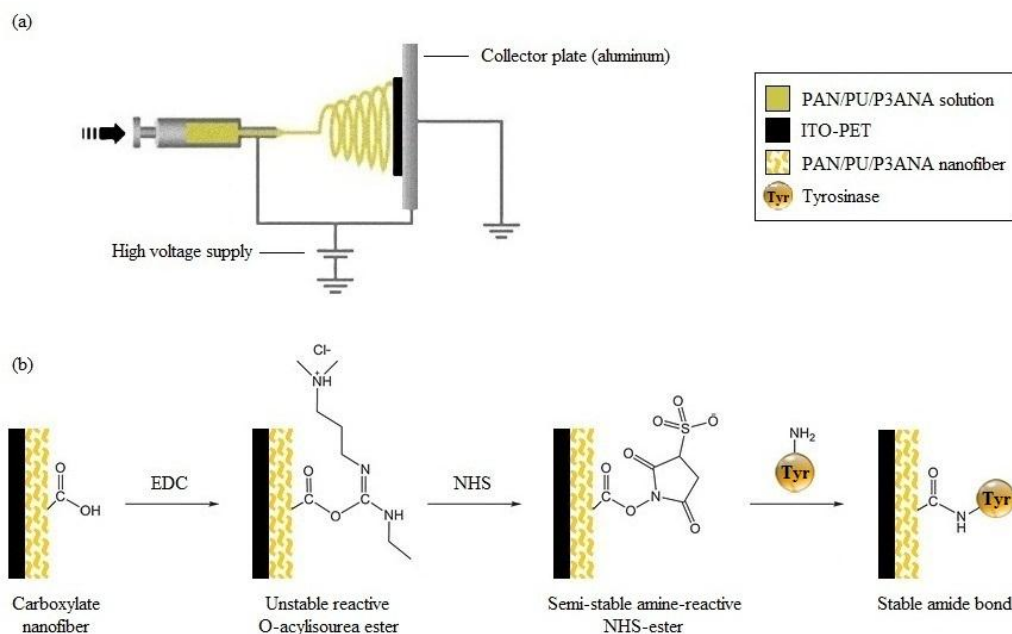


Figure 1.1 : Schematic representation of fabrication of PAN/PU/P3ANA nanofibers by electrospinning (a), and immobilization of tyrosinase onto nanofiber mat by EDC/NHS activation.

2. THEORETICAL PART

2.1 Conductive Polymers in Biosensor Applications

Conductive polymers exhibit electronic, magnetic, and optical properties comparable to metals or semiconductors. Hence, they are also referred to as “synthetic metals”. Their conductive behaviour arises from the delocalization of π -bonded electrons along the polymeric backbone, yielding high electron affinity and low ionization potential [27].

Their favorable charge transport properties and their sensitivity to even minor perturbations have made conductive polymers versatile tools in bioanalytical science, especially in biosensor applications. Design and fabrication of new biosensor systems are facilitated by the recent developments in controlled synthesis and further modification of these polymeric materials. They are susceptible to doping, and also serve as effective matrices for immobilization of biomolecules such as enzymes, antibodies, neurotransmitters or nucleic acids. This endows them with unique catalytic properties required of a promising biosensor design. Furthermore, when blended with another suitable polymer, conductive polymers are also electrospinnable and nanofibers of conductive polymers present an even more effective matrix material as their porous structure eliminates the problem of limited mass transfer, significantly reducing the response time of the biosensor [27].

The most noteworthy conductive polymers used in biosensor applications are polypyrrole, polythiophene, poly(3,4-ethylenedioxythiophene), polycarbazole, polyaniline and their derivatives. Among these, polyaniline (PANI) and its derivatives stand out as the better alternative due to their enhanced electrochemical properties, redox recyclability, ease of doping, good environmental stability and ease of preparation. There are, however, some limitations to its use because of its poor solubility in the most common solvents and its inadequate mechanical strength. But, these limitations are overcome by the carboxyl functionalized derivative of polyaniline which is named polyanthranilic acid (PANA). Ability to control its

doping level through an acid doping/ base dedoping process made it unique among the conjugated polymers. Besides, it possesses free carboxyl groups in its structure onto which enzymes can covalently bind, and that makes polyanthranalic acid even more favorable to employ in biosensor fabrication procedure [27].

2.2 Electrospinning

Electrospinning is a technique employed in production of fine fibers, with diameters of down to nanometer scale, from polymer solutions or melts. It is an electrostatic technique employing a high voltage electric field to charge the surface of a droplet of polymer solution, inducing the ejection of a liquid jet through a spinneret [28].

Basic set up of an electrospinning system consists of three components: a high voltage power supply, a spinneret, and a grounded collecting plate (Figure 1.1.a). An electric field is applied on the polymer solution at the tip of the capillary spinneret, inducing an electric charge on the liquid surface. When the applied electric field reaches a critical value, the surface tension forces holding the liquid are overcome by the repulsive electrical forces, ejecting a charged jet of solution from the tip of the Taylor cone. During the rapid transfer of the charged jet from the tip of the spinneret to the collector plate, the solvent evaporates and the polymer left behind is collected on the plate, in the form of interconnected web of fibers [28].

2.2.1 Effects of various parameters on electrospinning process

For an electrospinning process to work efficiently, there are certain parameters to be taken into account. These parameters can mainly be classified as solution parameters and process parameters. Solution parameters include concentration, molecular weight, viscosity, surface tension, and conductivity, whereas process parameters are applied voltage, feed rate, and tip-to-collector distance [28].

All these parameters have significant effect on the fiber morphology, therefore, proper optimization is required to obtain fibers of desired diameters and morphology [28].

2.2.1.1 Concentration

Fiber formation requires a moderate solution concentration. It has been observed that low solution concentrations result in a mixture of fibers and beads. As the solution

concentration increases, spherical beads become spindle-like, gradually turning into uniform fibers of increasing diameters. But, there is also an upper limit because, in high concentrations, the difficulty to maintain the solution flow at the needle tip hinders the continuous fiber formation [28].

2.2.1.2 Molecular weight

Molecular weight of the polymer indicates the degree of entanglement of the polymer chains, so it is correlated with other parameters such as viscosity, surface tension and conductivity. It has been found that polymers of high molecular weight usually result in desirable viscosity for fiber formation, whereas low molecular weight polymer solutions tend to form beads rather than fibers [28].

2.2.1.3 Viscosity

Solution viscosity is directly related with polymer concentration and the molecular weight of the polymer, and likewise, it has a considerable effect on fiber size and morphology. Too low viscosity does not promote continuous fiber formation. Increasing viscosity facilitates the formation of uniform fibers, whereas in the case of too high viscosity ejection of charged jets from polymer solution is hindered [28].

2.2.1.4 Surface tension

Since surface tension determines the critical point that needs to be overcome by repulsive electrical forces, it plays an important role in electrospinning process. Electrospinning of a polymer solution with lower surface tension can occur at a lower electric field. Low surface tension also promotes formation of bead-free fibers. Surface tension is the dominant factor especially for the solutions of low viscosity [28].

2.2.1.5 Conductivity / surface charge density

Jet formation is mainly directed by the charged ions in the polymer solution as they increase the charge carrying capacity of the jet and, in turn, subject it to higher tension under the applied electric field. Increased electrical conductivity has been observed to result in a decrease in fiber diameter, however, highly conductive solutions are extremely unstable under strong electric field and this leads to a broad diameter distribution [28].

2.2.1.6 Applied voltage

Applied voltage is an important parameter considering it is one of the governing factors in reaching the threshold voltage for fiber formation to start, when the necessary charge induction is provided under electric field. But the exact way in which the voltage affects the electrospinning process has not yet been agreed upon. It has been suggested that higher voltages promote more polymer ejection, leading to formation of fibers of larger diameters, whereas it has been reported by other authors that higher voltages cause an increase in electrostatic repulsive forces and promotes the formation of fibers of smaller diameters [28].

2.2.1.7 Feed rate / flow rate

The flow rate of the solution within the syringe affects the transfer rate of the polymer and, in turn, the jet velocity. Sufficient time for the evaporation of the solvent is required, therefore the feed rate should rather be kept low, otherwise beaded fibers are formed [28].

2.2.1.8 Tip to collector distance

Similar to the feed rate, tip to collector distance is also important for providing enough time for the solvent to evaporate before reaching the collector plate. Furthermore, it was reported that closer distance promotes formation of flatter fibers whereas they become rounder as the distance increases [28].

2.3 Dopamine

Dopamine is an electroactive neurotransmitter of the catecholamine family, produced in certain brain areas and adrenal glands through decarboxylation of DOPA (Figure 2.1). Among the catecholamines taking part in brain-body integration regarding cognitive and behavioral functions, dopamine is the most abundant one, and it also serves as a precursor for adrenaline and noradrenaline, other neurotransmitters in mammalian central nervous system [29].

Dopamine is also the most versatile neurotransmitter, considering the various tasks it undertakes in the organism ranging from neuroplasticity, brain circuitry, regulation of stress responses to its effects on cardiovascular and renal systems, as well as on attention span, learning and memory. It holds the central role in the reward and

pleasure system of the brain, therefore, is directly associated with motivational behavior. This dopaminergic pleasure pathway is the same pathway which is activated by drugs of abuse, hence dopamine has been the focus of many studies on mechanisms of addiction. Furthermore, deviations from the optimal dopamine levels in the central nervous system has been found to be an indicator of several neurological disorders such as schizophrenia, Alzheimer's disease, Parkinson's disease, and attention deficit hyperactivity disorder (ADHD) [29].

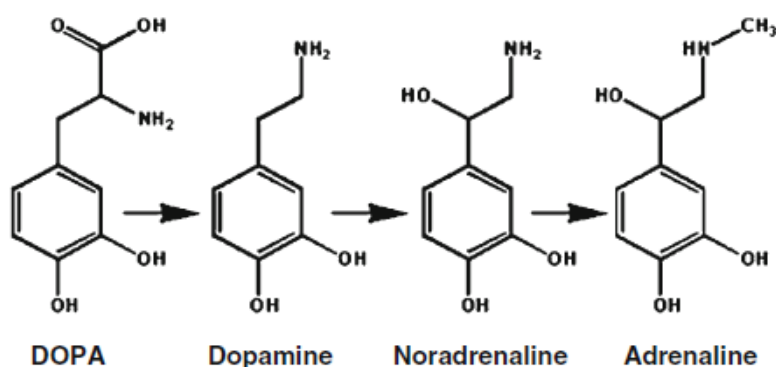


Figure 2.1 : Sequence of enzymatic reactions generating other catecholamines from L-DOPA.

Dopamine is also the most versatile neurotransmitter, considering the various tasks it undertakes in the organism ranging from neuroplasticity, brain circuitry, regulation of stress responses to its effects on cardiovascular and renal systems, as well as on attention span, learning and memory. It holds the central role in the reward and pleasure system of the brain, therefore, is directly associated with motivational behavior. This dopaminergic pleasure pathway is the same pathway which is activated by drugs of abuse, hence dopamine has been the focus of many studies on mechanisms of addiction. Furthermore, deviations from the optimal dopamine levels in the central nervous system has been found to be an indicator of several neurological disorders such as schizophrenia, Alzheimer's disease, Parkinson's disease, and attention deficit hyperactivity disorder (ADHD) [29].

Considering the advancement in disease diagnosis and treatment it promises, precise and accurate measurement of dopamine at the low levels (nanomolar scale or below) holds a clinical significance. There are numerous studies employing detection techniques such as liquid chromatography, mass spectroscopy, capillary electrophoresis and so on, but electrochemical sensing techniques offer the most

straightforward, cost-effective and rapid approach for detection of electroactive compounds [29].

2.4 Electrochemical Impedance Spectroscopy in Biosensor Applications

IUPAC defines electrochemical biosensors as “a self-contained integrated device, which is capable of providing specific quantitative or semi quantitative analytical information using a biological recognition element (biochemical receptor) which is retained in direct spatial contact with an electrochemical transduction element”. So, basically there are two essential components: a biochemical recognition element (e.g. enzymes, antibodies) to translate the input from the biochemical process into a physical or chemical output signal, and a transducer which, in turn, translates this signal into an electrical response. As for an electrochemical biosensor for dopamine detection, biological recognition element is the enzyme tyrosinase (Tyr), also known as polyphenol oxidase (PPO), which specifically binds to phenolic compounds, dopamine being one of them. Transducers for electrochemical biosensors are mostly based on amperometric detection which, simply, measures the current generated from oxidation or reduction of the electroactive analytes. This simple amperometric approach, however, has certain drawbacks such as relatively low output current density, background noise in the electrical response, and detrimental effect of the process on enzyme activity. On the other hand, transducers based on electrochemical impedance spectroscopy (EIS) offers a convenient, nondestructive, and versatile technique [29].

Electrochemical impedance spectroscopy is a powerful tool in biosensor applications, both in fabrication and detection processes. This technique analyzes the changes in interfacial properties of modified electrodes, resulting from the biorecognition process taking place at the surfaces. Formation of a recognition complex between the biological recognition element and the analyte molecule at the conductive or semiconductive transducer interface results in changes in electrical properties, such as capacitance or resistance. Measured impedance is the total result of each individual contribution from the solution, the support material, the sensing biomolecule, the working electrode and the counter electrode. Therefore, besides the consequent detection through the biorecognition process, a step-by-step analysis can reveal the effects of every single stage of surface modification process, such as the

effect of biomolecule immobilization on the transducer. Therefore, this makes electrochemical impedance spectroscopy an indispensable tool not only for detection, but for sensor optimization process as well, which is crucial for attaining high reactivity, stability, and avoidance of nonspecific interactions [29].

2.5 Basic Principles and Terms in Impedance Spectroscopy

The impedance of a system (Z) is measured by detecting the current response for an applied voltage perturbation of a small amplitude. It is a complex value because the change in current can occur both in terms of amplitude, and in terms of phase angle (ϕ) as well. Therefore, the impedance value can be expressed either by the modulus $|Z|$ with the phase shift ϕ , or by giving the real (Z_R) and imaginary (Z_I) parts of the impedance (Figure 2.2). The plot displaying $\log|Z|$ and ϕ as a function of logarithm of frequency ($\log f$) is termed as a Bode plot, and the plot displaying Z_R and Z_I is called a Nyquist plot [30].

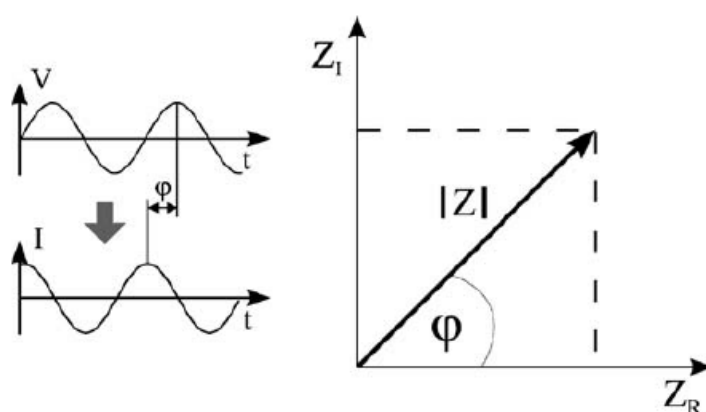


Figure 2.2 : Impedance expressed as the modulus $|Z|$ and the phase angle ϕ , or specified by the real (Z_R) and imaginary (Z_I) parts.

Impedance measurements are not performed at a single frequency value, it rather covers a wide frequency spectrum, so it is called spectroscopy. And this impedance spectrum allows the characterization of surfaces and layers, also giving information on exchange and diffusion processes. Furthermore, it simplifies the analytical comparison between different systems through detecting the frequency interval where the relative changes are the most noticeable [30].

To define the impedance behaviour of an electrolyte solution, usually four elements are referred. These are ohmic resistance, capacitance, constant phase element and Warburg impedance. These ideal or distributed impedance elements, in the

arrangements of series and/or parallel circuits, are employed in modelling equivalent circuits to approximate the experimental data with a fitting circuit model. This procedure allows for an in-depth analysis of the impedance behaviour for electrochemical systems [30].

Figure 2.3 displays a common equivalent circuit called Randles circuit which is applicable in the case of an electrode immersed in an electrolyte. This circuit consists of the solution resistance (R_s), the charge transfer resistance (R_{ct}), the double layer capacitance (C_{dl}), and the Warburg impedance (W) [30].

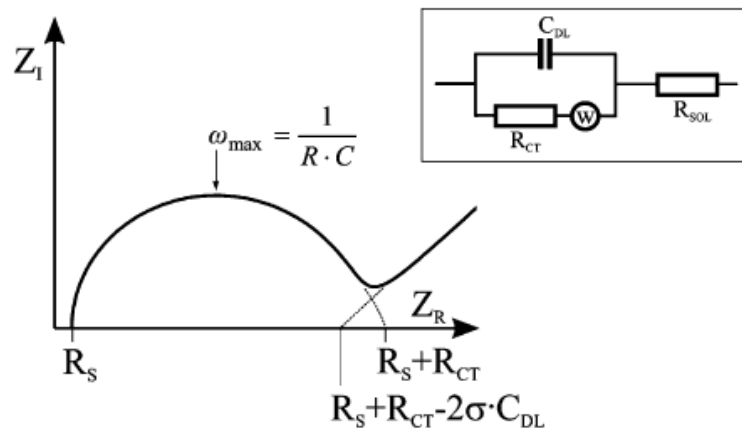


Figure 2.3 : Randles' equivalent circuit for an electrode in contact with an electrolyte.

R_s is correlated with the ion concentration and the cell geometry. R_{ct} arises from the current flow generated by redox reactions at the interface. C_{dl} refers to charge that is stored in the double layer at the interface and W comes from the impedance of the current as a result of diffusion from the bulk solution to the interface. R_s and R_{ct} values can be determined from the Nyquist plot, and using the frequency at the maximum of the semicircle, C_{dl} can also be calculated from the formula $\omega = 2\pi f = 1/R_{ct}C_{dl}$. The intercept obtained when the 45° line expressing Warburg-limited behaviour is extrapolated to the real axis equals to $R_s + R_{ct} - 2\sigma C_{dl}$, from which σ , hence the diffusion coefficients, can be derived [30].

3. EXPERIMENTAL PART

3.1 Materials

Polyacrylonitrile (PAN; $M_w = 150,000$ g/mol), 3-Aminobenzoic acid (m-anthranilic acid), Tyrosinase from mushrooms (EC 1.14.18.1), N-(3-Dimethylaminopropyl)-N'-ethylcarbodiimide hydrochloride (EDC) and N-Hydroxysuccinimide (NHS) were purchased from Sigma Aldrich. The bicinchoninic acid (BCA) Protein Quantitation Kit was obtained from Sigma Aldrich. Phosphate buffer saline (PBS) was obtained from Gibco. Dimethyl formamide (DMF Analytical Grade) were supplied from Merck (Germany). Poly(m-anthranilic acid) (P3ANA) was synthesized according to our previous study [a]. Briefly, 3-aminobenzoic acid (0.043 mol) has been dissolved in 90 ml of 0.5 M NaOH. Equal mole of ammonium persulfate in water (30 mL) has been added dropwise to this solution and the mixture was stirred at room temperature for 24 h. The precipitated polymer has been collected by filtration, washed with 1.2 M HCl and water until the filtrate became colorless and dried in vacuum at 60°C for two days. This polymer has been recovered in 70% yield as a brown powder. All of these chemicals were analytical grade and used as received.

3.2 Preparation of PAN/PU/P3ANA Blends

Polyacrylonitrile and polyurethane with a mass ratio of 1:1 were dissolved in dimethylformamide (DMF), stirring for 3 h at room temperature to obtain a homogeneous solution (6 wt%). Then, three samples of 5 ml were taken from this solution to add increasing amount of poly(m-anthranilic acid) (P3ANA) onto each one of them, 0.075 g, 0.15 g, 0.30 g, respectively, and stirred for another 2 h at room temperature.

3.3 Electrospinning of PAN/PU/P3ANA

Each electrospinning solution was taken into a syringe with a metal needle of 0.7 mm outer diameter which was connected to a high-voltage direct current (DC) power

supply (ES 30 Model Gamma High Voltage Inc., USA). The grounded counter electrode was connected to aluminum foil collector positioned at a distance of 15 cm from the needle tip. The flow rate of the solution, controlled by a syringe pump (NE-500 Model, New Era Pump Systems, Inc. USA), was kept at 1 ml/h and electrospinning was performed at 15 kV driving voltage. For reproducible electrochemical measurements, nanofibers of PAN/PU/P3ANA were obtained by collecting nanofibers onto ITO-PET (NV Innovative Sputtering Technology, Zulte, Belgium, PET 175 lm, Coating ITO-60) substrate with dimensions of 0.5 x 2.5 mm, for 5 minutes.

3.4 Covalent Immobilization of Tyrosinase onto Nanofiber Mats

Tyrosinase was immobilized onto the nanofiber mats by EDC/NHS activation procedure. Nanofiber mats on ITO-PET substrates were treated with 5 mL of EDC/NHS solution (1:1 molar ratio, 10 mg/ml in 0.1 M PBS buffer with pH 7.4) and shaken gently for 2 h at room temperature. Then the activated nanofiber mats were taken out and after being washed twice with PBS buffer, they were treated with tyrosinase solutions with 0.5mg/mL and 2 mg/mL concentrations, for another 2 h at 4°C, being shaken gently. Finally, they were taken out, washed twice again with PBS buffer and dried for characterization.

3.5 Quantification of Protein Amount on the Nanofiber Mats

The amount of immobilized tyrosinase on the nanofiber mats was determined by BCA protein assay. Initial tyrosinase solutions as well as the residual solution of each consecutive washing step were subjected to BCA assay to observe the gradual change in the amount of protein. The total protein content in each sample was calculated by comparing the means of absorption values with a standard curve of bovine serum tyrosinase dilutions (between 0 and 2mg/ml). The samples were incubated with BCA working solution at 37°C for 30 minutes and the absorbance was read at 562 nm by UV-Vis spectrophotometer (Perkin Elmer, Lambda 45) [31].

3.6 Structural, Morphological and Electrochemical Characterization

The structural properties of PAN/PU/P3ANA and tyrosinase immobilized nanofibers

were investigated by FTIR-ATR spectrophotometer (Perkin Elmer, Spectrum One, with a universal ATR attachment with a diamond and a ZnSe crystal). All FTIR-ATR spectra were collected with 12 scans in the 600-4000 cm^{-1} spectral region at 4 cm^{-1} resolution. The incorporation of P3ANA on the obtained nanofibers was analyzed by UV-Vis spectrophotometer. The structure, composition, and morphology of PAN/PU/P3ANA nanofibers were analyzed with SEM (Scanning Electron Microscopy)/EDX (Energy-Dispersive X-ray Spectroscopy) (QUANTA 400 F) before and after tyrosinase immobilization, with 10kV accelerating voltage after nanofiber mats were coated with gold by Ion Sputter Metal Coating Device (MCM-100 Model). Electrochemical measurements were performed in 0.1 M PBS using potentiostat 2263 Electrochemical Analyser (Princeton Applied Research, USA) with frequency range between 0.01 Hz and 100 kHz and AC voltage of 10 mV. Three-electrode system, consisting of nanofiber mat as working electrode, platinum wire as counter electrode, and silver wire as pseudo reference electrode, was used. All measurements were repeated three times for confirmation. The measured impedance spectra were analyzed in terms of electrical equivalent circuits using the analysis program ZSimpWin V.3.10.

4. RESULTS AND DISCUSSION

4.1 Spectroscopic Characterization of Nanofibers

UV-Vis spectroscopy was carried out to confirm the incorporation of each polymer in the blend, namely PAN, PU and P3ANA, into the nanofiber mats. UV-Vis spectra of PAN, PU and PAN/PU/P3ANA blend are given in Figure 4.1.

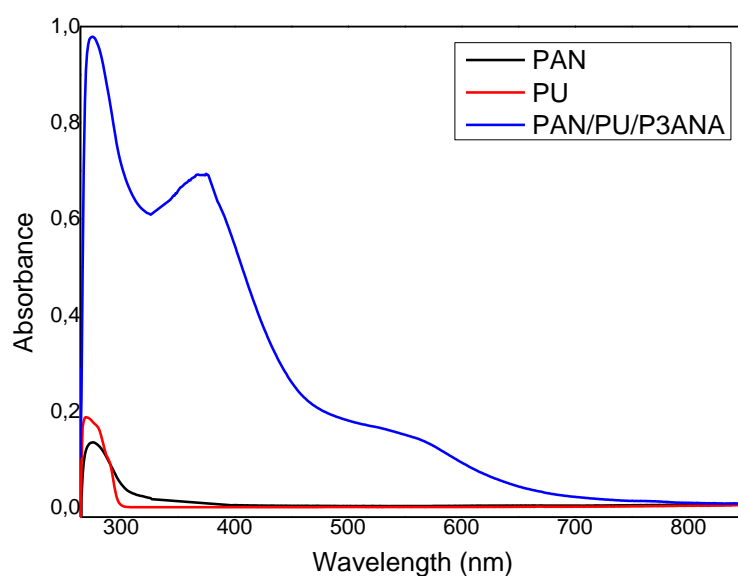


Figure 4.1 : UV-Vis spectra of PAN, PU, P3ANA and PAN/PU/P3ANA.

PAN nanofibers dissolved in DMF display an absorption band at 274 nm, which is characteristic for them due to $C\equiv N$ π -absorption [32]. In case of PU nanofibers dissolved in DMF, an absorption band around 270-280 nm is observed, which results from benzene π - π^* transitions [33]. Absorption bands obtained from PAN/PU/P3ANA nanofibers dissolved in DMF cover these characteristic bands for PAN and PU, besides, new bands are observed which are characteristic to P3ANA. The new band at 340–380 nm corresponds to π - π^* transition in benzene ring of poly(m-anthranilic acid). The broad band between 480 nm and 650 nm results from

the existence of polaron bands, which depends on the overall oxidation state of the polymer [19].

UV-Vis spectrophotometric data, which confirm the incorporation of each polymer into nanofiber mat, is further supported by subsequent FTIR-ATR analysis. FTIR spectra of PAN/PU/P3ANA nanofibers with increasing P3ANA amounts are given in Figure 4.2.

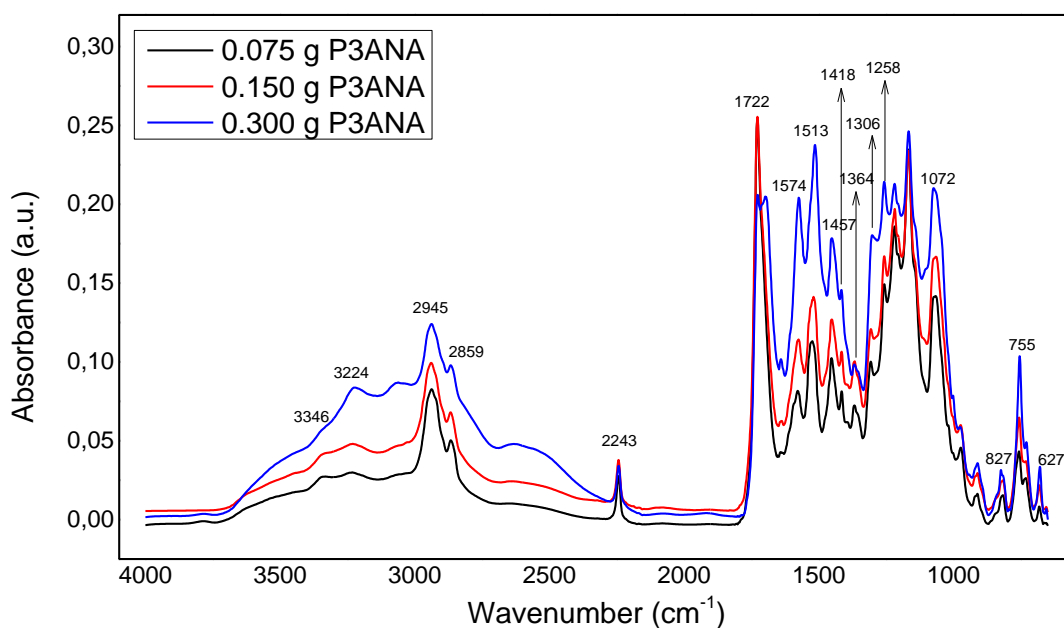


Figure 4.2 : FTIR spectra of PAN/PU/P3ANA blend with increasing P3ANA amounts.

PAN displays a characteristic peak at 2243 cm^{-1} , due to the $\text{--C}\equiv\text{N}$ stretching of acrylonitrile unit in the polymer chain. The peak at 2945 cm^{-1} indicates --CH stretching and bending vibrations, whereas the ones at 1364 and 1457 cm^{-1} are attributed to --CH in-plane deformation vibrations of CH_2 groups [34]. Regarding PU, a peak is observed at 3346 cm^{-1} , which is attributed to NH stretching. The peaks at 2931 and 2859 cm^{-1} are associated with --CH_2 stretching. The peak at 1722 cm^{-1} belongs to C=O group in polyurethane and the one at 1529 cm^{-1} to the group of NH vibrations. The ones at 1464 , 1418 , 1370 and 1306 cm^{-1} identify with the other modes of --CH_2 vibrations [35]. P3ANA in the blend displays a wide band between 3750 and 1800 cm^{-1} . The peaks observed at 3224 , 1693 , 1570 , 1507 cm^{-1} are

attributed to O-H stretching, C=O stretching, C=C stretching, N-H stretching, respectively. The ones at 1258 and 1077 cm^{-1} are due to C-N stretching and the ones at 827, 755, and 677 cm^{-1} belong to out-of-plane C-N stretching [19]. It can also be seen that the bands characteristic to P3ANA is intensified in correlation with increasing P3ANA amount in the blend.

As stated earlier, the carboxyl groups on P3ANA provide active sites for enzyme binding. In order to immobilize an enzyme onto -COOH containing surface, it is desirable to obtain a succinimidyl ester (-COOSuc)-terminated surface. The COOSuc surface of nanofiber mat was formed by reacting carboxyl groups of P3ANA with N-hydroxysuccinimide (NHS), in the presence of N-ethyl-N-(3-(dimethylamino)propyl) carbodiimide (EDC) [12]. The nanofiber mats which contain higher amount of P3ANA have more reactive groups (-COOH) and higher enzyme loading capacity. Therefore, nanofiber mat with 0.300 g P3ANA was chosen for immobilization of tyrosinase.

FTIR spectra of the enzyme immobilized nanofiber mats are given in Figure 4.3. As compared to the nanofibers which were not treated with enzyme solution, nanofibers with 0.5 mg tyrosinase displays a decrease in the intensity of certain peaks at 3063, 1640, 1573, 1520, 1454, 1256, 1215, and 1077 cm^{-1} . These peaks are characteristic to tyrosinase, therefore, they indicate the interaction between tyrosinase and nanofibers. It can also be noted that the intensity of these peaks decreased even further upon the addition of more tyrosinase. The one at 3063 cm^{-1} as well as the newly formed band at 3346 cm^{-1} corresponds to NH stretching vibrations. The peak at 1640 cm^{-1} is due to C=O stretching vibrations while the out-of-phase CN stretching vibrations have a minor contribution to it. 1573 and 1454 cm^{-1} are attributed to CC stretching vibrations, while CH bending vibrations also contribute to the band at 1454 cm^{-1} . The peak at 1520 cm^{-1} is a result of the combined effects of NH in plane bend and the CN stretching vibrations. The one at 1256 cm^{-1} is a result of C-O and CC stretching, whereas 1215 and 1077 cm^{-1} is due to NH bending vibrations [36, 37].

When tyrosinase immobilized onto PAN/PU/P3ANA nanofiber mat, the amino group (NH) of the tyrosinase and -COOH terminated surface reacts and a strong covalent peptide bond is formed. After immobilization of tyrosinase onto nanofiber mat, the peak at 3224 cm^{-1} which is attributed to O-H stretching of P3ANA is attenuated and a

new peak at 3346 cm^{-1} corresponding to NH stretching vibrations of tyrosinase was appeared. These results suggest covalent immobilization of tyrosinase.

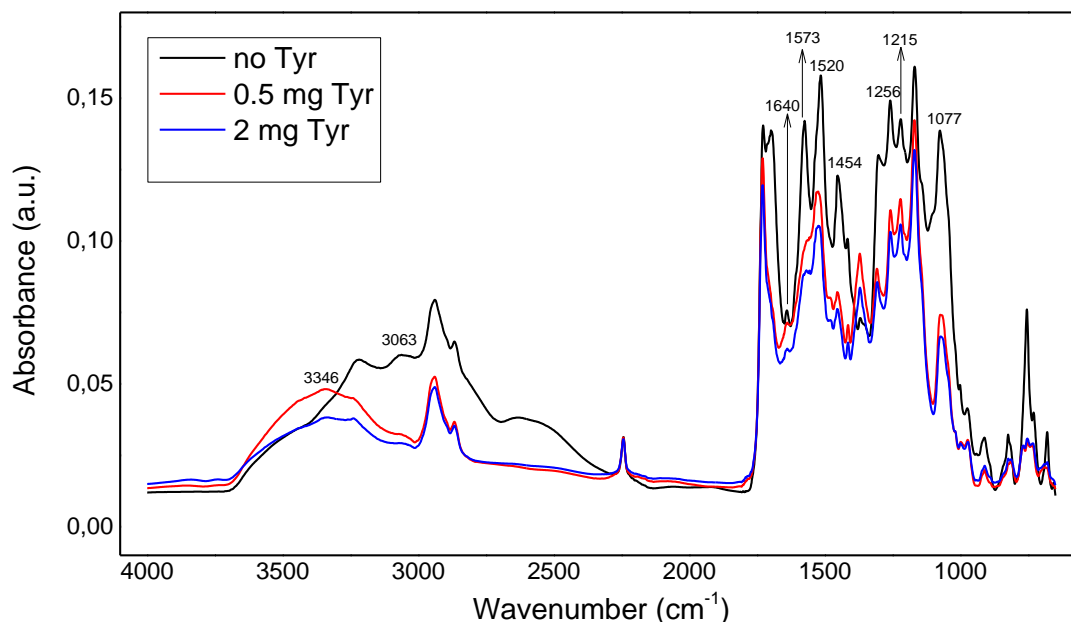


Figure 4.3 : FTIR-ATR spectra of tyrosinase immobilized PAN/PU/P3ANA nanofibers.

4.2 Determination of Immobilized Enzyme Amount by BCA Assay

The amount of immobilized tyrosinase on the PAN/PU/P3ANA nanofiber mats was determined by BCA protein assay. After each reaction run, the tyrosinase immobilized nanofiber mats were taken out and washed with PBS to remove any residual enzyme on the nanofiber mats. They were then reintroduced into a fresh reaction medium, and the enzyme amount was detected. Figure 4.4 shows the amount of initial and residual tyrosinase after each immobilization step. 2 mg and 0.5 mg of initial amounts tyrosinase were incubated with PAN/PU/P3ANA nanofiber mats. Figure 5 shows that after incubation, tyrosinase amount of the remaining solutions (green) were decreased to 0.15 mg and 0.046 mg for initial amounts of 2 mg and 0.5 mg, respectively. The difference between tyrosinase amounts of the initial solutions and solution obtained after binding process indicates that some of the protein is attached onto nanofibers. After two washing steps, there was only 0.012 mg and 0.00971 mg protein in the solution which represent the physically absorbed

tyrosinase. According to BCA results, 87% of the tyrosinase was bound to nanofibers covalently.

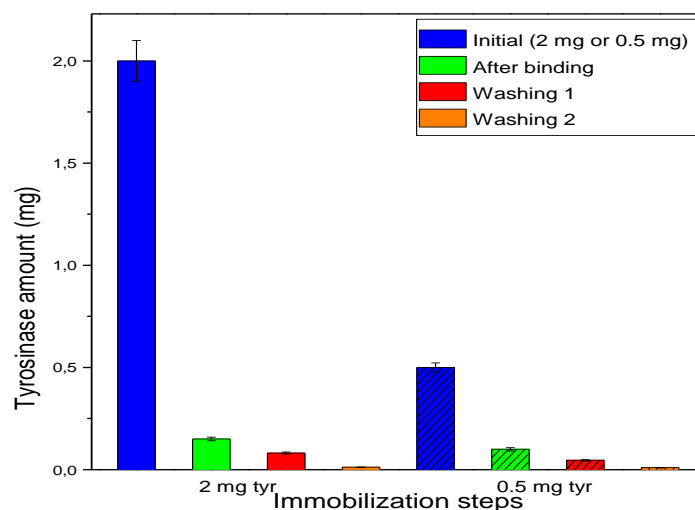


Figure 4.4 : Amount of initial and residual tyrosinase after each immobilization step.

4.3 Morphological Characterization of Nanofibers

The morphology of electrospun nanofibers, before (Figure 4.5) and after enzyme immobilization (Figure 4.6), are given below. The average diameters of PAN/PU nanofibers and PAN/PU/P3ANA nanofibers containing 0.075 mg, 0.150 mg and 0.300 mg of P3ANA were determined as 103 ± 11 nm, 144 ± 24 nm, 111 ± 17 nm and 119 ± 22 nm by ImageJ to randomly measure the diameters of 20 individual fibers shown in SEM images with $3\mu\text{m}$ magnification.

Nanofibers of PAN/PU display a relatively smooth surface. There is no considerable change in diameter upon the addition of P3ANA into the blend, however, the surface morphology of nanofibers changed substantially from smooth to rough. This transformation correlates with the change in the volatility of the solvent and the conductivity of the polymer solution due to P3ANA addition. Incorporation of P3ANA into the blend increases the charge density of the polymer solution, owing to its aminocarboxyl groups which promote a large charge accumulation. Self-repulsion of these excess charges under high electrical field generates stronger elongation forces on the jet. As a result, surface tension is more readily overcome, leading to an

increased volatility of the solvent. And rapid evaporation of the solvent, in turn, results in nanofibers with rough surfaces [19, 38, 39].

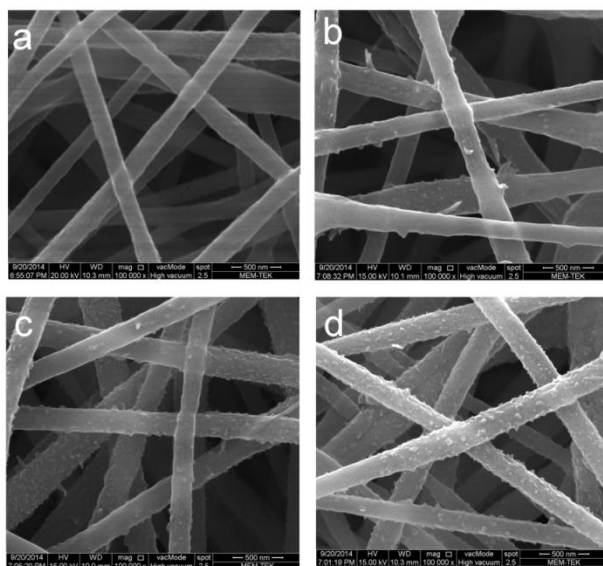


Figure 4.5 : SEM images of PAN/PU (a), and PAN/PU/P3ANA nanofibers containing 0.075 g (b), 0.150 g (c) and 0.300 g (d) of P3ANA

The amount of immobilized protein or enzyme is proportional to the roughness of the surface [40]. Therefore, the nanofiber mat of PAN/PU/P3ANA which contains 0.300 mg of P3ANA with the roughest surface is the most suitable one for tyrosinase immobilization.

In Figure 4.6, the average diameters of nanofibers after immobilization of 0.5 mg and 2 mg of tyrosinase, was 131 ± 22 nm and 141 ± 21 , respectively. It was observed that enzyme immobilization procedure resulted in an increase in fiber diameter. It can also be noted that these enzyme immobilized nanofibers (Figure 4.6.b,c) have rather smoother surfaces than those of neat PAN/PU/P3ANA nanofibers (Figure 4.6.a).

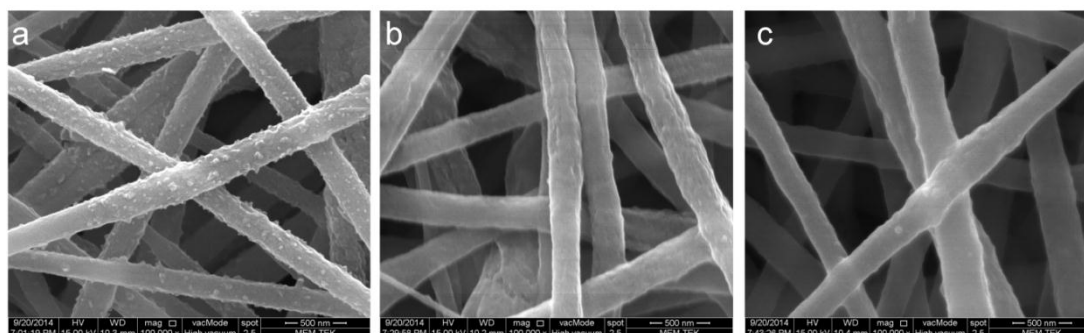


Figure 4.6 : SEM images of PAN/PU/P3ANA nanofibers (a) and 0.5 mg (b) and 2 mg (c) of tyrosinase immobilized nanofibers.

Although the increase in diameter and change in surface morphology indicates the binding of enzyme onto nanofibers, due to small size of the enzyme (approximately 25 nm [41]) there is a need for another analyses to confirm the binding of enzyme. Tyrosinase is a binuclear copper (Cu) containing metalloprotein [42], while none of the polymers in the nanofiber mat has Cu atom in their structure. The structure and composition of the tyrosinase immobilized nanofibers were analyzed by detection of elemental concentrations for nitrogen and copper with EDX. Also, in order to investigate the distribution of immobilized tyrosinase on the surface, EDX-mapping of PAN/PU/P3ANA nanofiber mats were performed (Figure 4.7).

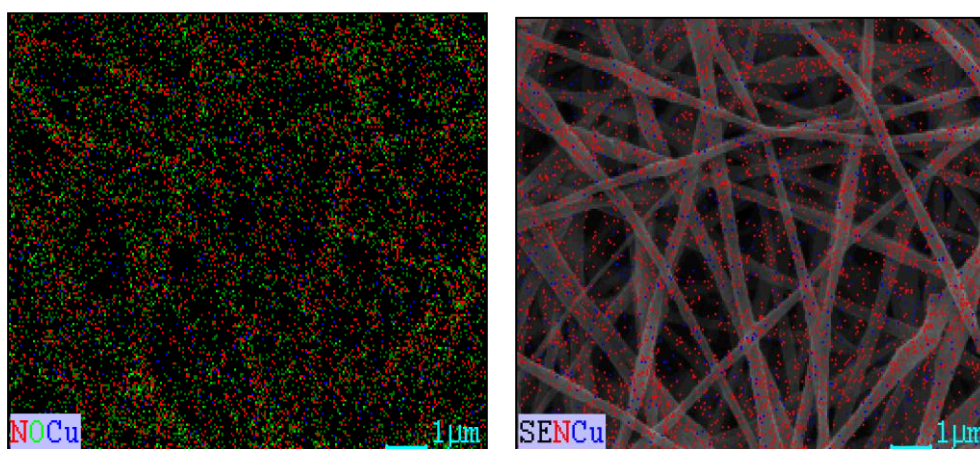


Figure 4.7 : EDX-mapping of nitrogen (red) and copper (Blue) atoms on the surface of tyrosinase immobilized PAN/PU/P3ANA nanofibers.

PAN/PU/P3ANA nanofiber mat possesses no Cu atoms in its structure. The amount of Cu (wt %) on the surface of nanofiber mats were increased with the increasing amount of immobilized tyrosinase. Also, this enzyme has nitrogen (N) atoms in its backbone, as well as P3ANA and PAN, so nitrogen atoms can be introduced to the structure through covalent immobilization of the enzyme. The amount of N atoms also increased with increasing amount of immobilized tyrosinase. The compositions of included atoms (nitrogen and copper) in the structure are given in Table 4.1.

EDX-mapping micrographs of tyrosinase immobilized nanofibers show the distribution of the immobilized enzyme (Figure 4.7). This micrograph indicates that the distribution of the enzyme on the surface of nanofibers is affected by the distribution of functional groups (-COOH) of P3ANA. The results obtained from

FTIR-ATR, BCA protein assay and SEM/EDX analyses have been complementary and able to verify the covalent immobilization of tyrosinase in increasing amounts.

Table 4.1 : Elemental concentrations for nitrogen and copper atoms in PAN/PU/P3ANA nanofibers and tyrosinase immobilized nanofibers.

Samples	Elements (wt %)	
	N	Cu
PAN/PU/P3ANA	20.93	-
0.5mg Tyrosinase	26.19	5.51
2mg Tyrosinase	26.66	5.88

4.4 Electrochemical Impedance Spectroscopy and Equivalent Circuit Modelling

Electrical properties of tyrosinase immobilized PAN/PU/P3ANA nanofibers on ITO-PET were determined by electrochemical impedance spectroscopy (EIS).

The EIS data provide information about the nature of electrochemical process occurring at the electrode/electrolyte interface [43]. The Nyquist (Figure 4.8.A) and Bode phase (Figure 4.8.B) plots of the PAN/PU/P3ANA nanofibers were recorded by applying AC signal of 10 mV amplitude in the frequency range 0.01 Hz to 100 kHz, before (no Tyr) and after tyrosinase (0.5mg and 2mg Tyr) immobilization. A significant difference in the impedance spectra was observed after covalent immobilization of tyrosinase onto nanofibers.

In Nyquist plot, PAN/PU/P3ANA nanofibers and tyrosinase immobilized nanofibers exhibited a semi-circle, and the diameter of the semi-circle become smaller with the immobilization of enzyme. Nanofibers of PAN/PU/P3ANA and tyrosinase immobilized have phase angle values of ~ 70 degrees. At medium to low frequency domain of Bode phase plot of tyrosinase immobilized nanofibers, changes in phase angle values were observed. These changes represent the presence of additional capacitive elements arising from immobilization of enzyme on the nanofiber surface [44]. The measured impedance spectra were analyzed in terms of electrical equivalent circuits to evaluate the kinetics of the systems using the analysis program ZSimpWin.

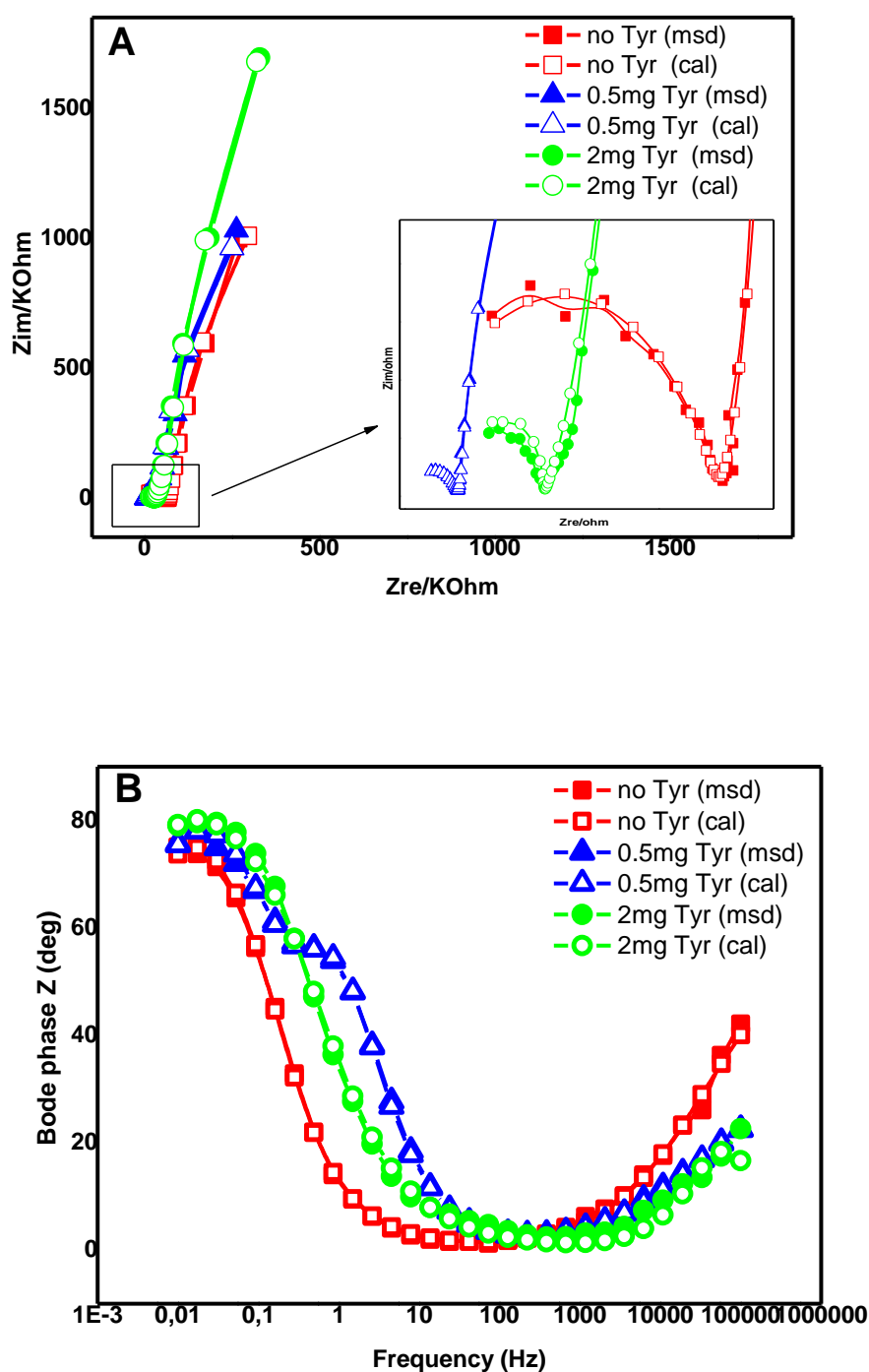


Figure 4.8 : Nyquist (A), and Bode Phase (B) plots indicating that measured and calculated data well fitted to each other with the model.

The circuits for PAN/PU/P3ANA nanofibers and tyrosinase immobilized nanofibers (PAN/PU/P3ANA-Tyr), which describe the physical properties of the system and provide a good fit to the measured data with a reasonable number of circuit elements,

were chosen. The calculated and measured data were fitted well together with the chosen equivalent circuits (Figure 4.9).

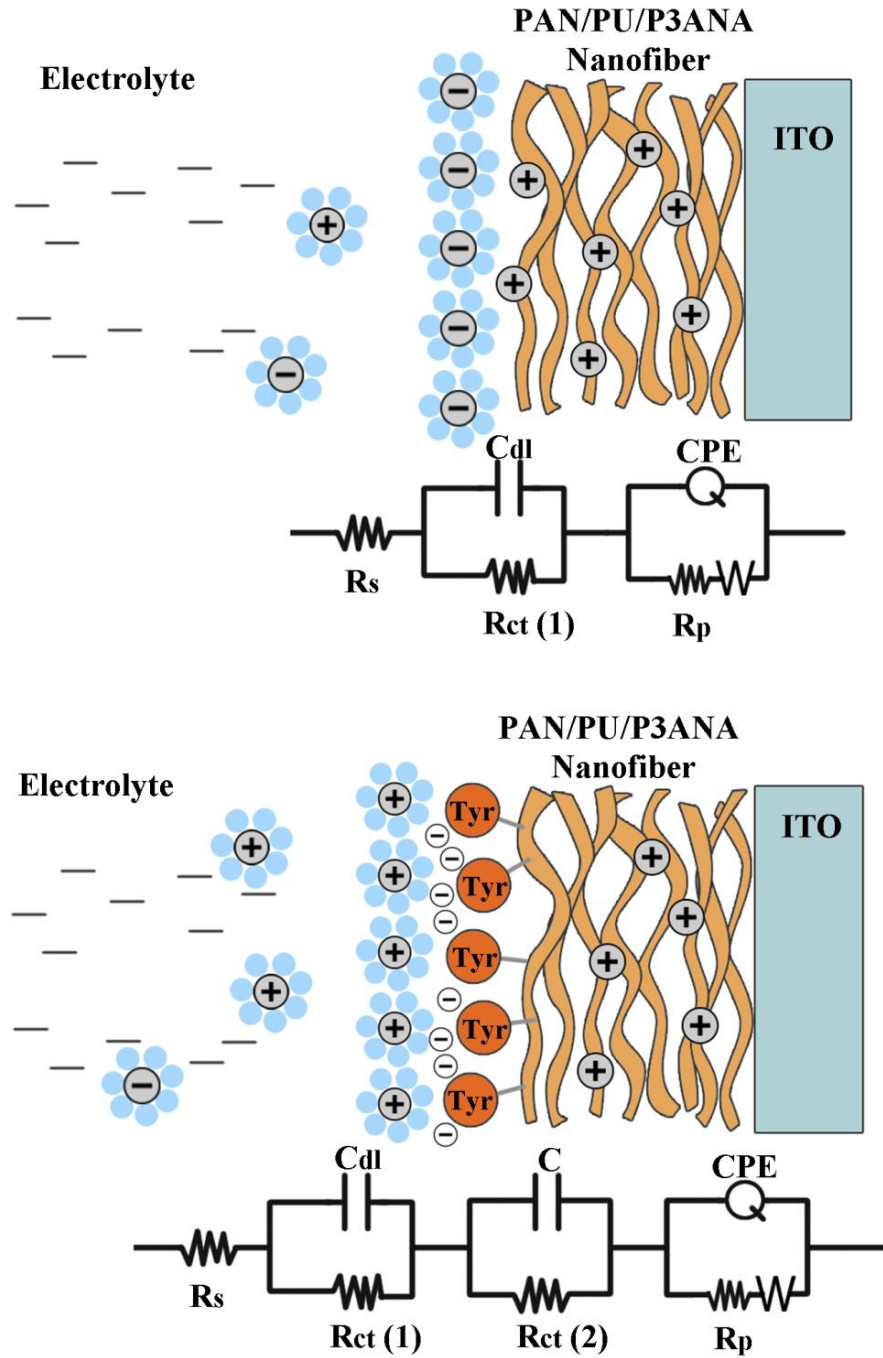


Figure 4.9 : Equivalent circuits for the simulation of the EIS spectra of PAN/PU/P3ANA nanofibers (top) and tyrosinase immobilized PAN/PU/P3ANA nanofibers (bottom).

The impedance spectra for nanofibers (PAN/PU/P3ANA) described by the equivalent circuit of $R(CR)(QR)W$ (Figure 4.9) in short hand. For PAN/PU/P3ANA-Tyr, the equivalent circuit of $R(CR)(CR)(QR)W$ were selected since there are

additional electrical components (resistance and capacitance) arise from immobilized tyrosinase. In Figure 4.9, the first component of two circuits, R_s , represents the solution resistance of the electrolyte. The solution resistance corresponds to the Ohmic resistance due to the presence of the electrolyte on the nanofiber and in solution [19] and of electrical contacts [45]. R_s values for PAN/PU/P3ANA nanofibers, 0.5 mg and 2 mg of tyrosinase immobilized nanofibers were $1.00 \times 10^{-7} \Omega$, $1.12 \times 10^{-10} \Omega$ and $1.21 \times 10^{-11} \Omega$, respectively. The R_s values correspond to the behavior of the electrolyte, filling pores of nanofibers [46]. It is obvious from the SEM images that the surfaces of tyrosinase immobilized nanofibers are smoother than PAN/PU/P3ANA nanofibers. So it is expected to have higher solution resistance for PAN/PU/P3ANA nanofibers. The second resistance in both circuits represents the charge transfer resistance (R_{ct}) between the solution and the surface of the modified (tyrosinase) or unmodified nanofiber electrode surface. C_{dl} corresponds to double layer capacitance along nanofiber mats. First C_{dl} elements arise from alignment of solvated counter ions along electrode surface. The electron transfer through electrode occurs by overcoming activation barrier, charge transfer resistance and solution resistance [47]. For tyrosinase immobilized PAN/PU/P3ANA nanofibers (Figure 4.9.b), the second $C(2)$ and $R_{ct}(2)$ which are connected in parallel to first ones, represent the capacitance and the charge transfer resistance between immobilized enzyme molecules and nanofibers, respectively. Q represents the constant phase element (CPE). CPE was applied in the equivalent circuit for the simulation of the impedance data. CPE takes into account the non homogeneity of the conductance [19] and the electrode [45]. The impedance of such a non-ideal electrode is defined by the formula of ($Z_{CPE} = TCPE(j\omega)^{-n}$) where $TCPE$ and n are frequency-independent constants; ω is the angular frequency [43], n is a parameter describing the deviation from an ideal capacitor and arises from the slope of the $\log Z$ versus $\log f$ plot. The values for n vary from 0 to 1. $n = 1$ subscribes to an ideal capacitor, while $n=0$ and 0.5, denotes a resistance and Warburg behavior, respectively [48]. W represents the Warburg impedance and it is attributed to the diffusion of counter-ions. Once the electron transfer begins, the electrode kinetics determined by Warburg impedance (W) due to the mass transport [47]. R_p represents the pore resistances of the nanofiber layer (Ohmic resistances of the electrolyte in the pores) [49]. Table 4.2 represents the fitting parameters for the equivalent circuit elements by modelling of the impedance spectra in Figure 4.8. Double layer capacitance (C_{dl}) along the surface

of nanofibers showed no significant change after immobilization tyrosinase (C_{dl}). The charge transfer resistance (R_{1ct}) of $2.62 \times 10^6 \Omega$ of PAN/PU/P3ANA nanofibers decreased to R_{1ct} of $2.47 \times 10^6 \Omega$ and $1.5 \times 10^2 \Omega$ after immobilization of 0.5 mg and 2 mg tyrosinase, respectively. The isoelectric point (pI) of tyrosinase lies at pH=6.1. Since all the EIS measurements were performed in PBS buffer solution with a pH 7, the net charge of tyrosinase is slightly negative [50]. The concentrations of ions in PBS buffer electrolyte have been reported [51]. For PBS electrolyte (100 mM, pH 7.5, $T = 25^\circ\text{C}$), the concentrations of negative ions such as $[\text{H}_2\text{PO}_4^-]$, $[\text{H}_2\text{PO}_4^{2-}]$, $[\text{PO}_4^{3-}]$ and $[\text{OH}^-]$ are approximately 100 mM. However, the concentrations of positive ions such as $[\text{Na}^+]$ and $[\text{H}^+]$ are approximately 170 mM. These values refer to the bulk electrolyte and its total positive charge concentration is greater than negative charge concentration. Positively charge ions interact with negatively charged tyrosinase and solvated counter ions align along the nanofiber surface.

The capacitance (C) occurring at the interphase between immobilized enzyme and nanofibers decreased while charge transfer resistance R_{ct} (2) increased. Since negatively charged ions are relatively bigger compared to positively charged ions, their transfer through positively charge P3ANA containing nanofiber becomes challenging. Also these ions can be repulsed by tyrosinase. The difference between capacitance values of tyrosinase immobilized nanofibers can also be explained by the different interfacial structures, assuming different structures or sizes [52].

The n value of PAN/PU/P3ANA nanofiber was 0.65 and it slightly reduced with tyrosinase immobilization. The values for $n=0.5$ donates Warburg behavior. It is also an indicative of electrode surface structure. For value of n, zero indicates that the electrode is not porous, while 1 means that the electrode has a porous structure [53]. Since enzyme immobilized nanofibers become smoother, it is expected to observe lower n values with the increasing amount of tyrosinase. Charge transfer resistance between solution and the surface of nanofibers decreased with enzyme immobilization when the porosity and homogeneity of the electrode decreased. Also, with immobilization of tyrosinase, pore resistance (R_p) decreased compared to PAN/PU/P3ANA nanofibers. However, R_p increased with the increasing amount of tyrosinase onto nanofibers. These differences in R_p can be explained by the fact that covalent immobilization of tyrosinase by EDC/NHS activation forms a different nanofiber mat structure [54].

Table 4.2 : Fitting values for the equivalent circuit elements by the simulation of the impedance spectra in Figure 4.9.

	PAN/PU/P3ANA	0.5mg Tyrosinase	2mg Tyrosinase
Circuit notation	R(CR)(QR)W	R(CR)(CR)(QR)W	
Rs (Ω)	1.00E-7	1.12E-10	1.21E-11
C_{dl} (F)	3.21E-5	3.26E-5	3.17E-5
R_{ct}(1) (Ω)	2.62E6	2.47E6	1.50E2
C (F) (10^{-5})	-	2.64	1.96
R_{ct}(2) (Ω)	-	1.55E4	6.34E6
Q (CPE) (10^{-7}) (Ω^{-1})	0.10	1.41	0.42
R_p (Ω)	30800	4514	14300
W (10^5) (Ssec⁵/cm²)	10.64	24.06	5.57
n	0.65	0.57	0.53
Chi-squared error	6.921E-04	7.025E-04	1.072E-03

CONCLUSION

PAN/PU/P3ANA nanofiber mats with varying P3ANA amounts were successfully fabricated. Data obtained by UV-visible spectroscopy and FTIR-ATR displayed the incorporation of each polymer in the blend into the nanofiber mats. Nanofiber mats with the highest amount of P3ANA were then used for tyrosinase immobilization, since P3ANA presents the carboxyl groups for covalent binding of the enzyme, therefore, higher amount of P3ANA yields an increased enzyme loading capacity. Spectroscopic data obtained by FTIR-ATR and BCA assay confirmed that covalent enzyme immobilization by EDC/NHS activation procedure was successful. The surface of the tyrosinase immobilized PAN/PU/P3ANA nanofibers became smooth and the diameters of the fibers increased by about 50 nm. Elemental analyses and EDX-mapping of nitrogen and copper atoms showed that the distribution of the enzyme on the surface of nanofibers is affected by the distribution of functional groups (-COOH) of P3ANA. The electrochemical behaviors of nanofibers significantly changed with enzyme immobilization depending on the changes in morphology of nanofibers and charges of enzyme and P3ANA. The solution resistance and charge transfer resistance of nanofibers decreased after enzyme immobilization.

REFERENCES

- [1] Wang, Z. G., Wan, L. S., Liu, Z. M., Huang, X. J., Xu, Z. K. (2009). Enzyme immobilization on electrospun polymer nanofibers: an overview, *Journal of Molecular Catalysis B: Enzymatic*, **56**, 189-195.
- [2] Polat, T., Bazin, H. G., & Linhardt, R. J. (1997). Enzyme catalyzed regioselective synthesis of sucrose fatty acid ester surfactants, *Journal of Carbohydrate Chemistry*, **16**, 1319-1325.
- [3] Hasan, F., Shah, A. A., Hameed, A. (2006). Industrial applications of microbial lipases, *Enzyme and Microbial Technology*, **39**, 235-251.
- [4] Choudhary, G., Wu, S. L., Shieh, P., Hancock, W. S. (2003). Multiple enzymatic digestion for enhanced sequence coverage of proteins in complex proteomic mixtures using capillary LC with ion trap MS/MS, *Journal of Proteome Research*, **2**, 59-67.
- [5] Akgöl, S., Dinçkaya, E. (1999). A novel biosensor for specific determination of hydrogen peroxide: catalase enzyme electrode based on dissolved oxygen probe, *Talanta*, **48**, 363-367.
- [6] Ju, K. S., Parales, R. E. (2006). Control of substrate specificity by active-site residues in nitrobenzene dioxygenase, *Applied and Environmental Microbiology*, **72**, 1817-1824.
- [7] Wołosowska, S., Synowiecki, J. (2004). Thermostable β -glucosidase with a broad substrate specificity suitable for processing of lactose-containing products, *Food Chemistry*, **85**, 181-187.
- [8] Adelt, S., Podeschwa, M., Dallmann, G., Altenbach, H. J., Vogel, G. (2003). Stereo- and regiospecificity of yeast phytases—chemical synthesis and enzymatic conversion of the substrate analogues neo- and L-chiro-inositol hexakisphosphate, *Bioorganic Chemistry*, **31**, 44-67.
- [9] Seeger, M., Zielinski, M., Timmis, K. N., & Hofer, B. (1999). Regiospecificity of dioxygenation of di- to pentachlorobiphenyls and their degradation to chlorobenzoates by the bph-encoded catabolic pathway of Burkholderia sp. strain LB400, *Applied and Environmental Microbiology*, **65**, 3614-3621.
- [10] Ericksen, S. S., Szklarz, G. D. (2005). Regiospecificity of human cytochrome P450 1A1-mediated oxidations: the role of steric effects, *Journal of Biomolecular Structure and Dynamics*, **23**, 243-256.
- [11] Ye, P., Xu, Z. K., Wu, J., Innocent, C., Seta, P. (2006). Nanofibrous poly(acrylonitrile-co-maleic acid) membranes functionalized with gelatin and chitosan for lipase immobilization, *Biomaterials*, **27**, 4169-4176.
- [12] Sam, S., Touahir, L., Salvador Andresa, J., Allongue, P., Chazalviel, J. N., Gouget-Laemmel, A. C., Djebbar, S. (2009). Semiquantitative study

of the EDC/NHS activation of acid terminal groups at modified porous silicon surfaces, *Langmuir*, **26**, 809-814.

- [13] **Wan, L. S., Ke, B. B., Wu, J., Xu, Z. K.** (2007). Catalase immobilization on electrospun nanofibers: effects of porphyrin pendants and carbon nanotubes, *The Journal of Physical Chemistry C*, **III**, 14091-14097.
- [14] **Fernandes, K. F., Lima, C. S., Pinho, H., Collins, C. H.** (2003). Immobilization of horseradish peroxidase onto polyaniline polymers, *Process Biochemistry*, **38**, 1379-1384.
- [15] **Védrine, C., Fabiano, S., Tran-Minh, C.** (2003). Amperometric tyrosinase based biosensor using an electrogenerated polythiophene film as an entrapment support, *Talanta*, **59**, 535-544.
- [16] **Gerard, M., Chaubey, A., Malhotra, B. D.** (2002). Application of conducting polymers to biosensors, *Biosensors and Bioelectronics*, **17**, 345-359.
- [17] **Ahuja, T., Mir, I. A., Kumar, D.** (2007). Biomolecular immobilization on conducting polymers for biosensing applications, *Biomaterials*, **28**, 791-805.
- [18] **Chaubey, A., Pande, K. K., Singh, V. S., Malhotra, B. D.** (2000). Co-immobilization of lactate oxidase and lactate dehydrogenase on conducting polyaniline films, *Analytica Chimica Acta*, **407**, 97-103.
- [19] **Giray, D., Balkan, T., Dietzel, B., Sezai Sarac, A.** (2013). Electrochemical impedance study on nanofibers of poly (m-anthranilic acid)/polyacrylonitrile blends, *European Polymer Journal*, **49**, 2645-2653.
- [20] **Paul, E. W., Ricco, A. J., Wrighton, M. S.** (1985). Resistance of polyaniline films as a function of electrochemical potential and the fabrication of polyaniline-based microelectronic devices, *The Journal of Physical Chemistry*, **89**, 1441-1447.
- [21] **Wu, M. S., Wen, T. C., Gopalan, A.** (2002). In situ UV-visible spectroelectrochemical studies on the copolymerization of diphenylamine with anthranilic acid, *Materials Chemistry and Physics*, **74**, 58-65.
- [22] **Nguyen M.T., Diaz A. F.** (1995). Water-soluble poly(aniline-co-o-anthranilic acid) copolymers, *Macromolecules*, **28**, 3411-3415.
- [23] **Gorji, M., Jeddi, A., Gharehaghaji, A. A.** (2012). Fabrication and characterization of polyurethane electrospun nanofiber membranes for protective clothing applications, *Journal of Applied Polymer Science*, **125**, 4135-4141.
- [24] **Sizgek, G. D., Griffith, C. S., Sizgek, E., Luca, V.** (2009). Mesoporous zirconium titanium oxides, part 3, synthesis and adsorption properties of unfunctionalized and phosphonate-functionalized hierarchical polyacrylonitrile-F-127-templated beads, *Langmuir*, **25**, 11874-11882.
- [25] **Lu, Y., Tighzert, L., Dole, P., Erre, D.** (2005). Preparation and properties of starch thermoplastics modified with waterborne polyurethane from renewable resources, *Polymer*, **46**, 9863-9870.

- [26] **Wang, Z. G., Ke, B. B., Xu, Z. K.** (2007). Covalent immobilization of redox enzyme on electrospun nonwoven poly (acrylonitrile-co-acrylic acid) nanofiber mesh filled with carbon nanotubes: a comprehensive study, *Biotechnology and Bioengineering*, **97**, 708-720.
- [27] **Ates, M.** (2013). A review study of (bio)sensor systems based on conducting polymers, *Materials Science and Engineering C*, **33**, 1853-1859.
- [28] **Bhardwaj, N., Kundu, S. C.** (2010). Electrospinning: a fascinating fiber fabrication technique, *Biotechnology Advances*, **28**, 325-347.
- [29] **Jackowska, K., Kryszinski, P.** (2013). New trends in the electrochemical sensing of dopamine, *Analytical and Bioanalytical Chemistry*, **405**, 3753-3771.
- [30] **Lisdat, F., Schafer, D.** (2008). The use of electrochemical impedance spectroscopy for biosensing, *Analytical and Bioanalytical Chemistry*, **391**, 1555-1567.
- [31] **Ficen, S. Z., Guler, Z., Mitina, N., Finiuk, N., Stoika, R., Zaichenko, A., Ceylan, S. E.** (2013). Biophysical study of novel oligoelectrolyte based nonviral gene delivery systems for mammalian cells, *The Journal of Gene Medicine*, **15**, 193-204.
- [32] **Ge, J. J., Hou, H., Li, Q., Graham, M. J., Greiner, A., Reneker, D. H., Harris, F. W., Cheng, S. Z. D.** (2004). Assembly of well-aligned multiwalled carbon nanotubes in confined polyacrylonitrile environments: electrospun composite nanofiber sheets, *Journal of the American Chemical Society*, **126**, 15754-15761.
- [33] **Raghu, A. V., Jeong, H. M., Kim, J. H., Lee, Y. R., Cho, Y. B., Sirsalmath, K.** (2008). Synthesis and characterization of novel polyurethanes based on 4-((4-Hydroxyphenyl)iminomethyl)phenol, *Macromolecular Research*, **16**, 194-199.
- [34] **Ouyang, Q., Cheng, L., Wang, H., Li, K.** (2008). Mechanism and kinetics of the stabilization reactions of itaconic acid-modified polyacrylonitrile, *Polymer Degradation and Stability*, **93**, 1415-1421.
- [35] **Asefnejad, A., Khorasani, M. T., Behnamghader, A., Farsadzadeh, B., Bonakdar, S.** (2011). Manufacturing of biodegradable polyurethane scaffolds based on polycaprolactone using a phase separation method: physical properties and in vitro assay, *International Journal of Nanomedicine*, **6**, 2375-2384.
- [36] **Barth, A.** (2007). Infrared spectroscopy of proteins, *Biochimica et Biophysica Acta*, **1767**, 1073-1101.
- [37] **Naidja, A., Violante, A., Huang, P. M.** (1995). Adsorption of tyrosinase onto montmorillonite as influenced by hydroxialuminum coatings, *Clays and Clay Minerals*, **43**, 647-655.
- [38] **Cai, Y., Gao, D., Wei, Q., Gu, H., Zhou, S., Huang, F., Song, L., Hu, Y., Gao, W.** (2011). Effects of ferric chloride on structure, surface morphology and combustion property of electrospun polyacrylonitrile composite nanofibers, *Fibers and Polymers*, **12**, 145-150.

- [39] **Yu, D. G., Williams, G. R., Gao, L. D., Bligh, S. W. A., Yang, J. H., Wang, X.** (2012). Coaxial electrospinning with sodium dodecylbenzene sulfonate solution for high quality polyacrylonitrile nanofibers, *Colloids and Surfaces A: Physicochemical and Engineering Aspects*, **396**, 161-168.
- [40] **Acton, Q. A.** (2011). *Advances in Bionanotechnology Research and Application*, Scholarly Editions, Georgia.
- [41] **Hunter, C.** (2011). Supramolecular chemistry: bigger and better synthesis, *Nature*, **469**, 39-41.
- [42] **Wang, X., Chen, L., Xia, S., Zhu, Z., Zhao, J., Chovelon, J. M., Renaul, N. J.** (2006). Tyrosinase biosensor based on interdigitated electrodes for herbicides determination, *International Journal of Electrochemical Science*, **1**, 55-61.
- [43] **Gu, H., Su, X. D., Loh, K. P.** (2005). Electrochemical impedance sensing of DNA hybridization on conducting polymer film-modified diamond, *The Journal of Physical Chemistry B*, **109**, 13611-13618.
- [44] **De Crombrughe, A., Yunus, S., Bertrand, P.** (2008). Grafting and characterization of protein on polyaniline surface for biosensor applications, *Surface and Interface Analysis*, **40**, 404-407.
- [45] **Zehani, N., Dzyadevych, S. V., Kherrat, R., Jaffrezic-Renault, N. J.** (2014). Sensitive impedimetric biosensor for direct detection of diazinon based on lipases, *Frontiers in Chemistry*, **2**, 1-7.
- [46] **Radecka, M., Wierzbicka, M., Rekas, M.** (2004). Photoelectrochemical cell studied by impedance spectroscopy, *Physica B: Condensed Matter*, **351**, 121-128.
- [47] **Park, J. Y., Park, S. M.** (2009). DNA hybridization sensors based on electrochemical impedance spectroscopy as a detection tool, *Sensors*, **9**, 9513-9532.
- [48] **Lu, X., Dou, H., Yuan, C., Yang, S., Hao, L., Zhang, F., Zhang, X.** (2012). Polypyrrole/carbon nanotube nanocomposite enhanced the electrochemical capacitance of flexible graphene film for supercapacitors, *Journal of Power Sources*, **197**, 319-324.
- [49] **Panić, V. V., Dekanski, A. B., Mišković-Stanković, V. B., Nikolić, B. Ž.** (2009). The study of capacitance change during electrolyte penetration through carbon-supported hydrous ruthenium oxide prepared by the sol-gel procedure, *Chemical and Biochemical Engineering Quarterly*, **23**, 23-30.
- [50] **Gormally, M. V., McKibben, R. K., Johal, M. S., Selassie, C. R.** (2009). Controlling tyrosinase activity on charged polyelectrolyte surfaces: a QCM-D analysis, *Langmuir*, **25**, 10014-10019.
- [51] **Birner, S., Uhl, C., Bayer, M., Vogl, P.** (2008). Theoretical model for the detection of charged proteins with a silicon-on-insulator sensor, *Journal of Physics: Conference Series*, **107**, 012002.
- [52] **Kityakarn, S., Pooarporn, Y., Songsiriritthigul, P., Worayingyong, A., Robl, S., Braun, A. M., Wörner, M.** (2012). (Photo) Electrochemical

characterization of nanoporous TiO₂ and Ce-doped TiO₂ sol–gel film electrodes, *Electrochimica Acta*, **83**, 113-124.

- [53] **Rodríguez-Sevilla, E., Ramírez-Silva, M. T., Romero-Romo, M., Ibarra-Escutia, P., Palomar-Pardavé, M.** (2014). Electrochemical quantification of the antioxidant capacity of medicinal plants using biosensors, *Sensors*, **14**, 14423-14439.
- [54] **Pauliukaite, R., Ghica, M. E., Fatibello-Filho, O., Brett, C.** (2010). Electrochemical impedance studies of chitosan-modified electrodes for application in electrochemical sensors and biosensors, *Electrochimica Acta*, **55**, 6239-6247.

CURRICULUM VITAE



Name Surname: Uğur DAĞLI
Place and Date of Birth: Kırklareli, 29.12.1988
E-Mail: dagliu@itu.edu.tr
B.Sc.: Molecular Biology and Genetics, ITU